Physicochem. Probl. Miner. Process., 61(2), 2025, 204336

http://www.journalssystem.com/ppmp

Physicochemical Problems of Mineral Processing

ISSN 1643-1049

Adsorption mechanism of dodecyl phosphoric acid and dodecyl phosphate on kaolinite surface: DFT calculation and experimental verification

Shaowen Peng [1], Lingyun Liu [1,2], Chuilei Kong [1], Fangqin Lu [1], Hao Cheng [1]

[1] Department of Materials Science and Engineering, Anhui University of Science and Technology, Huainan 232001, China
[2] State Key Laboratory of Digital Intelligent Technology for Unmanned Coal Mining, Anhui University of Science and Technology

Correspongding author: lyunliu@163.com (Lingyun Liu)

Abstract: This study systematically investigates the adsorption mechanisms of dodecyl phosphoric acid (DDPA) and dodecyl phosphate (DPA) on the kaolinite (001) and (00$\bar{1}$) surfaces using density functional theory (DFT) simulations. Adsorption energy, differential charge density, Mulliken population, and density of states analyses reveal that both collectors exhibit significantly stronger adsorption on the (001) surface than on the (00$\bar{1}$) surface. DDPA forms hydrogen bonds on both surfaces, whereas DPA forms stable hydrogen bonds only on the (001) surface. Flotation experiments further confirm that, at collector concentrations below 1 mmol/L, DPA exhibits superior selective adsorption on kaolinite with particle sizes of 125-75 μm and demonstrates better separation selectivity in kaolinite-quartz mixtures. The experimental results are highly consistent with the DFT predictions.

Keywords: dodecyl phosphoric acid, dodecyl phosphate, kaolinite, density functional theory, adsorption mechanism

1. Introduction

Kaolinite is one of the main components in coal slime water and has important uses in biology, environmental protection, new materials, and other aspects (Li et al., 2023; Chi et al., 2017). In the current process of wet coal washing and processing, a large amount of coal slime water is produced (Chen et al., 2019; Morsy et al., 2014), and the coal slime water is mixed with a large number of fine particles of kaolinite (Müller et al., 2020). The existence of minerals such as kaolinite not only affects the yield and grade of flotation clean coal but also seriously affects the dewatering of flotation tailings, which has also become a hot topic of concern for scholars. Therefore, the separation of kaolinite from coal slime water is of great significance for the clarification treatment of highly argillized coal slime water and the processing and utilization of kaolinite.

At present, fine kaolinite is mainly separated from minerals by flotation, so there are many studies on the collector reagents for kaolinite flotation (Zhou et al., 2022; Yang S et al., 2014). In recent years, many scholars have studied the flotation behavior of kaolinite. Many researchers have been committed to studying and developing new types of cationic collectors to improve the flotation behavior of kaolinite. Among them, amine collectors have a better adsorption effect on kaolinite (Ma et al., 2009). Liu et al. (2018) found through the research on the aggregation behavior of kaolinite particles by cationic, anionic and nonionic surfactants that the aggregation effect of kaolinite particles in the presence of cationic surfactants was significantly better than that in anionic and nonionic surfactants, and the adsorption capacity of dodecylamine on the surface of kaolinite was greater than that of oleic acid. Liu et al. (2015) studied the effects of particle size and the chain length of reagents on the flotation of kaolinite by quaternary ammonium salt through flotation experiments. However, these reagents are mainly used for separating kaolinite in bauxite and not mainly for collecting kaolinite in coal slime water (Long et al., 2015). The crystal structure of kaolinite is a triclinic system, with specific lattice

DOI: 10.37190/ppmp/204336

constants and angles. The (001) and (00$\bar{1}$) planes of kaolinite are important surfaces of the kaolinite crystal (Ma et al., 2023; Šolc et al., 2011), and its crystal structure is composed of connected Si-O tetrahedra and Al-O octahedra, and the structural layers are stacked along the c-axis. The interlayers of kaolinite are strengthened by strong hydrogen bonds (O-OH = 0.289 nm), and the stacking mode is that adjacent structural layers are mutually staggered by 1/3 a along the a-axis, with rotations at different angles, resulting in different polytypes of kaolinite. In the actual structure, due to the deformation of Al-OH and the difference in size from the Si-O tetrahedron, the tetrahedron must undergo a slight relative rotation and warping to adapt to the Al-OH sheet. The crystal structure of quartz is composed of Si-O tetrahedra, each Si atom is surrounded by four O atoms, and the tetrahedra are connected through the vertices to form a three-dimensional framework structure. The layered structural characteristics of kaolinite and quartz reflect the differences in their respective chemical compositions and crystal structures, resulting in differences in the surface properties of the two minerals.

Therefore, it is necessary to find a reagent that can perform targeted adsorption on the (001) surface of kaolinite and have no adsorption or weak adsorption on the (00$\bar{1}$) surface of kaolinite, which is of great significance for the separation of kaolinite from coal slime water. Studies have shown that phosphoric acid has a certain activation effect on the surface of kaolinite. The activation of phosphoric acid is used to replace the more commonly used polymerization of dehydrated kaolinite and undehydrated kaolinite (Zhang et al., 2020). Kaolinite has better floatability under neutral conditions, while quartz has better floatability at pH = 12 (Ali et al., 2019; Zhou et al., 2022). Some ions, such as Ca^{2+}, have little effect on the floatability of kaolinite, but can improve the floatability of quartz at pH = 12 (Hou et al., 2020). The ACA study shows that kaolinite activated by phosphoric acid has higher reactivity and an increased specific surface area (Alvarez et al., 2024). Liu's research shows that the higher the iron (Fe) content in kaolinite, the better the adsorption behavior of sodium oleate on kaolinite (Liu et al.,2024). W Liu's research shows that the adsorption behavior of reagents on minerals is closely related to the charge size of the O atom on the reagent head group (Liu et al., 2019).

Phosphonic acid agents are easily combined with kaolinite. Therefore, DDPA and DPA were selected for flotation experiments and research in this paper (Sprankle et al., 1975). Experiments were carried out using different concentrations of agents for minerals of different particle size grades, and the results were analyzed to confirm whether DDPA and DPA have selectivity for the flotation of kaolinite and quartz, thereby determining the application prospects of the agents for the recovery of kaolinite.

2. Sample preparation and test methods

2.1. Material preparation

The high-purity kaolinite and quartz used in the experiment were respectively from Huaibei Jinyan Coal Measures Kaolin Co Ltd in Anhui Province and Henan Minghai Environmental Protection Technology Co Ltd. The mineral samples were crushed, ground and sieved, and then four particle size grades of 500 – 250 μm, 250 – 125 μm, 125 – 75 μm and 75 – 45 μm were obtained respectively for the experiment.

DPA was purchased from Jiangsu Aikon Biopharmaceutical R&D Co Ltd in China, and DDPA was purchased from Shanghai Macklin Biochemical Technology Co Ltd in China. All the reagent solutions in the experiment were freshly prepared and used immediately. The prepared reagent concentration was 100 mmol. During use, the concentration of the mixed solution was controlled by adding different volumes. All the water used in the experiment was deionized water.

2.2. Test method

2.2.1. Single mineral flotation test

In this experiment, the XFG-35II type flotation machine produced by Changsha Instrument and Equipment Co., Ltd. was used. For each group of experiments, 10.000 ±0.001 g of kaolinite and quartz samples were weighed respectively using an analytical balance and placed into the flotation cell. Then, the corresponding volume of deionized water was added to the flotation cell. After adding the deionized water, the mixture was stirred for 2 minutes on the flotation machine to evenly disperse the minerals in the water. The DDPA and DPA collectors were added, respectively, and then the solutions

were made to reach different concentrations. After adding the collectors, the mixture was stirred for 3 minutes to fully mix the minerals and the reagents. Then, the aeration valve of the flotation machine was opened to start froth scraping, and the froth scraping time was 3 minutes. The rotation speed of the flotation machine was 2400 r/min. After the flotation, the concentrate and tailings were dried and weighed. The recovery rate calculation formula is as follows:

$$P = \frac{m_1}{m_1+m_2} \times 100\% \quad (1)$$

In the formula, P represents the flotation yield, %; $m1$ is the mass of the concentrate, g; $m2$ is the mass of the tailings, g.

2.2.2. Flotation test of kaolinite - quartz mixed minerals

The operation steps of the flotation test of the kaolinite-quartz mixed system are as follows: Firstly, the two minerals are mixed in different proportions. The percentage of kaolinite is determined according to the aluminum-silicon ratio in the mixed sample. The flotation steps are the same as those of the single mineral, and the calculation of the flotation recovery rate is also the same as that of the single mineral flotation recovery rate. In the kaolinite-quartz mixed mineral system, the grade of the flotation concentrate is mainly judged by different proportions. The specific operations are as follows:

A series of kaolinite-quartz mixed samples with different proportions was configured. XRF analysis was conducted on each sample to determine the contents of Al_2O_3 and SiO_2. The standard curve diagram of concentrate grade was obtained by using the ratio of Al_2O_3/SiO_2 and the content of kaolinite-quartz, as shown in Fig. 1. Next, a kaolinite-quartz mixed sample with a mass ratio of 1:1 was configured. Flotation tests of DDPA and DPA in the kaolinite-quartz mixed system were carried out at different concentrations of 1 mmol/L, 2 mmol/L, 3 mmol/L, 4 mmol/L, and 5 mmol/L. XRF analysis was conducted on the flotation concentrates to determine the contents of Al_2O_3 and SiO_2. Then, the mass percentage of kaolinite in the flotation concentrate, that is, the grade of the flotation concentrate, was determined according to the corresponding standard curve based on the ratio of Al_2O_3/SiO_2.

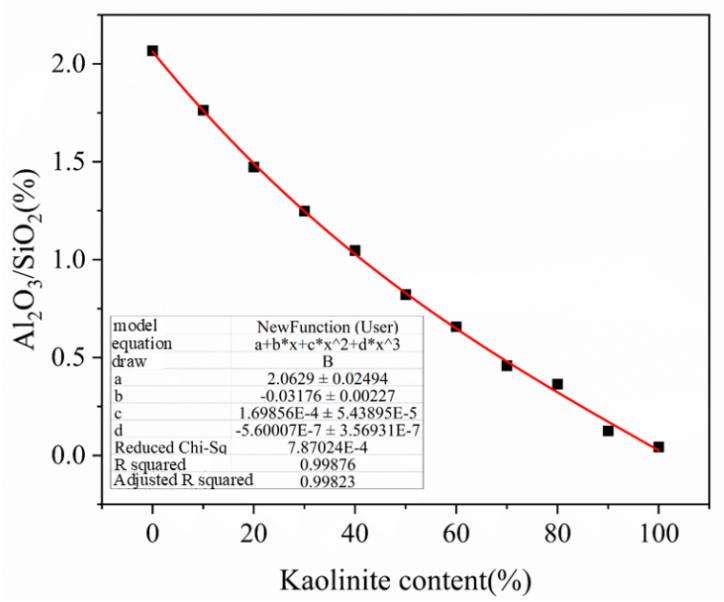

Fig. 1. The standard curve of concentrate grade in the kaolinite-quartz system

2.2.3. Fourier Transform Infrared Spectroscopy (FTIR)

The FTIR spectra of the samples were measured at room temperature (25 ± 2 °C) using a Nicolet 740 FTIR spectrometer in the wavenumber range of 400 to 4000 cm−1 on a KBr pellet. Before the measurement, kaolinite and quartz were ground to < 15 μm using an agate mortar. Then, a 1 g sample of the concentrate kaolinite after single mineral flotation was added to 30 mL aqueous solution with a pH value of 6.65 and adjusted for 0.5 h. Subsequently, the sample was filtered, washed three times with deionized water, and dried in a vacuum oven at 35 °C for 24 hours.

3. Simulation calculation

3.1. Computational details

The density functional calculations of DDPA and DPA on different layers of kaolinite were performed using the CASTEP module in Materials Studio 2019 software. The exchange-correlation function for the lattice geometry optimization of the kaolinite bulk phase was the GGA-PBE function, and the plane wave cutoff energy was set to 400 eV. The ultrasoft pseudopotential was used to describe the interaction between valence electrons and ions. The BFGS algorithm was used to optimize the model and calculate the properties, and the self-consistent field convergence accuracy was set to 2.0×10^{-6} eV/atom. The van der Waals force in the density functional calculation process was corrected using the Tkatchenko-Scheffler (TS) method. The convergence criteria for geometric optimization: the maximum atomic displacement was 0.2 pm, the interatomic force was 0.05 eV/A, the interatomic internal stress was 0.1 GPa, the total energy change of the system was 2.0×10^{-5} eV/atom, the smearing value used for the density of states analysis was 0.2 eV; all calculations were performed in the reciprocal space. OTAC+ was placed in a 2 nm × 2 nm × 4 nm periodic unit cell for optimization, and the Gamma point was selected for the Monkhorst-Pack grid k-point (Segall et al., 2022; Clark et al., 2005).

3.2. Calculation method of adsorption energy

Through the calculation of adsorption energy, the difficulty degree of adsorption of the adsorption reagent on the surface model and the relative stability of adsorption can be analyzed. When the adsorption energy is negative, it indicates that the adsorption reagent can spontaneously adsorb on the mineral surface, and the smaller the negative value, the more stable the adsorption. The calculation formula of the adsorption energy (E_{ads}) of the reagent adsorbed on the kaolinite surface is as follows:

$$E_{ads} = E_{total} - (E_{surface} + E_{adsorbate}) \quad (2)$$

In the formula, E_{total} represents the total energy of the system after the reagent is adsorbed on the surface of kaolinite, $E_{surface}$ represents the energy of the kaolinite surface before adsorption, and $E_{adsorbate}$ represents the energy of the reagent monomer before adsorption.

3.3. Model construction

Based on the similarity of the molecular structure of the kaolinite $(00\bar{1})$ surface and the quartz surface, in this paper, the kaolinite $(00\bar{1})$ surface was innovatively replaced by the quartz surface in the simulation process. By constructing the adsorption models of the reagent on the kaolinite (001) and $(00\bar{1})$ surfaces, the microscopic adsorption mechanism of the reagent on the kaolinite and quartz surfaces was explored, providing a new method for improving the grade of kaolinite in a multiphase complex mineral system.

Based on the frontier orbital theory, the smaller the absolute value of the energy difference (ΔE_1 or ΔE_2) between the HOMO orbital of one reactant and the LUMO orbital of the other reactant, the stronger the interaction between these two orbitals, and the more favorable for adsorption (Kamachi et al, 2019). The frontier orbital calculations of the surface model, DDPA, and DPA were carried out using the Dmol3 module, as shown in Table 1.

Table 1. Calculate the energy difference of the frontier orbitals of DDPA and DDA with the (001) and (001 bar) kaolinite surfaces

model	Frontier orbital energy eV)		DDPA		DPA	
	HOMO	LUMO	ΔE_1	ΔE_2	ΔE_1	ΔE_2
K(001)	-0.27461	-0.07079	-0.17774	0.27849	-0.18056	0.269063
K$(00\bar{1})$	-0.2667	-0.07151	-0.17703	0.270578	-0.17985	0.261151
DDPA	-0.24854	0.003883	\	\	\	\
DPA	-0.25135	-0.00554	\	\	\	\

The data show that the HOMO orbitals of DDPA and DPA are more likely to adsorb on the (001) surface and (00$\bar{1}$) surface of kaolinite than the LOMO orbitals, and are mainly concentrated at the head groups of the reagent molecules (Fig. 2). Among them, DDPA has three strongly electronegative O atoms, and DPA has four strongly electronegative O atoms, with the average charges of -0.605 e and -0.596 e, respectively. Numerous studies have shown that during energy minimization and dynamic relaxation, these molecules tend to transition toward more vertically oriented configurations (Prates et al, 2025). This conformational evolution significantly alters the adsorption energy landscape, reflecting the competition between van der Waals interactions and hydrophilic-hydrophobic effects (Zhang et al, 2020). Notably, on silica surfaces, which are inherently more hydrophobic than alumina, this transition promotes the alignment of polar moieties perpendicular to the surface, thereby enhancing molecular anchoring through hydrophobic interactions (Liu et al). Therefore, the adsorption model is constructed vertically, adsorbing the reagent head groups on the mineral surface (Lu et al, 2024; Bechthod et al, 2024).

The molecular arrangement on the (001) and (00$\bar{1}$) surfaces of kaolinite is highly symmetrical. Based on the atomic structure characteristics of the head groups of the reagents, the surface of kaolinite is divided into three sites, namely H1, H2, and H3 (Fig. 3). Meanwhile, each adsorption site can be divided into three adsorption modes according to different rotation angles of the reagents. Therefore, there are a total of nine adsorption sites, namely H1-1, H1-2, H1-3, H2-1, H2-2, H2-3, H3-1, H3-2, and H3-3.

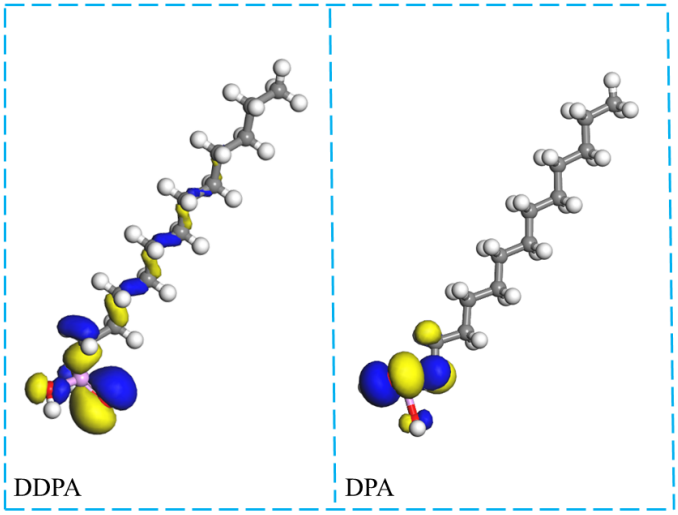

Fig. 2. Schematic diagram of the frontier orbitals of DDPA and DPA

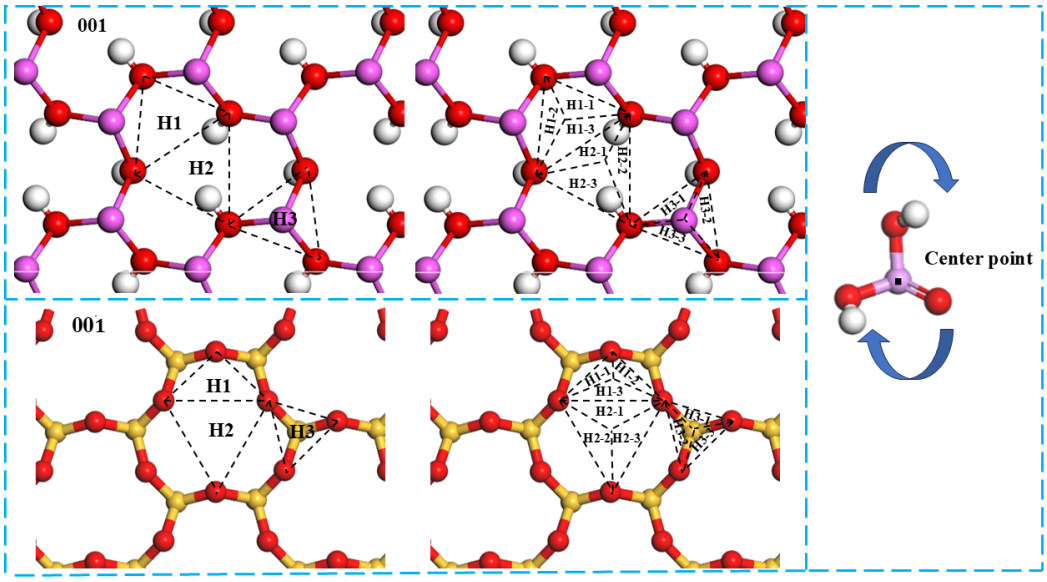

Fig. 3. Construction of adsorption sites of the (001) surface and (00$\bar{1}$) surface model of kaolinite

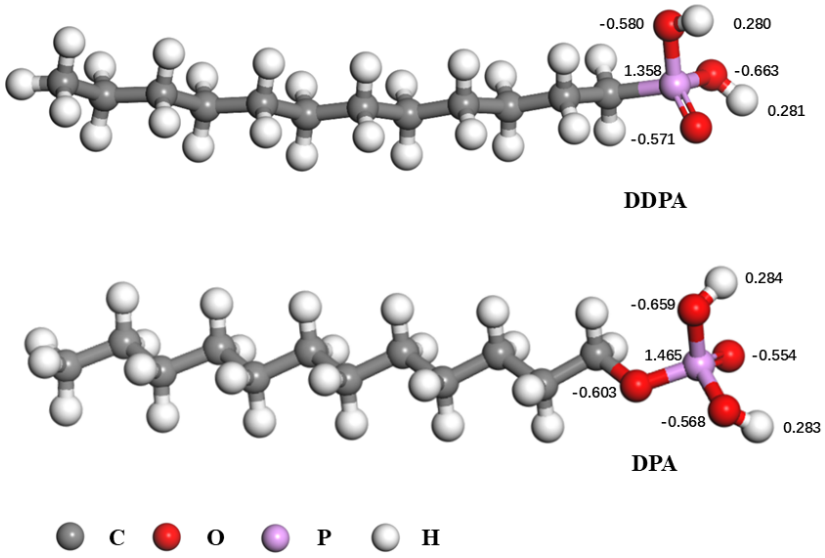

Fig. 4. Molecular structures of DDPA and DPA

4. Results and Discussion

4.1. Simulation calculation

4.1.1. Adsorption energy and stable adsorption configuration

As shown in Table 2 and 3, the adsorption energies of DDPA and DPA on the (001) and (00$\bar{1}$) surfaces of kaolinite are presented, respectively, and the lower the adsorption energy, the better the adsorption effect. It can be known from Table 1 that the adsorption energy of DDPA on the (001) surface of kaolinite is all lower than -95.73 kJ/mol, and the adsorption energy on 6 adsorption sites is lower than -112.23 kJ/mol. Among them, the adsorption energy on the adsorption site H2-1 is the lowest, which is -147.92 kJ/mol. However, the adsorption energy of DDPA at the H3-1 adsorption site on the (00$\bar{1}$) surface of kaolinite is the lowest, being -47.43 kJ/mol. On the whole, the adsorption energies at each adsorption site are much higher than those on the (001) surface of kaolinite. It can be known from Table 2 that the adsorption energy of DPA on the (001) surface of kaolinite is all lower than -81.18 kJ/mol, and the adsorption energy on 7 adsorption sites is lower than -122.48 kJ/mol. Among them, the adsorption energy on the adsorption site H3-1 is the lowest, which is -152.38 kJ/mol. The lowest adsorption energy point of DPA on the (00$\bar{1}$) surface of kaolinite is the H2-1 site, which is -46.78 kJ/mol. On the whole, each adsorption energy is much larger than that on the (001) surface of kaolinite. It can be seen that the adsorption of DDPA and DPA on the (001) surface of kaolinite is much stronger than that on the (00$\bar{1}$) surface of kaolinite, and the adsorption of DPA on the (001) surface of kaolinite is more stable than that of DDPA.

The stable adsorption configurations of DDPA at the optimal adsorption site H2 to 1 on the (001) surface of kaolinite and at the optimal adsorption site H3-1 on the (00$\bar{1}$) surface are shown in Fig. 5. For the hydrogen bond analysis, it can be seen that on the (001) surface of kaolinite, DDPA is mainly adsorbed by forming three hydrogen bonds through the O atoms in the molecule and the H atoms on the surface of the Al-OH group, namely O145-H15, O146-H34 and O84-H90. While on the (00$\bar{1}$) surface of kaolinite, it is mainly adsorbed by forming two hydrogen bonds through the H atoms in the DDPA molecule and the O atoms on the Si-O group, namely O39-H58 and O41-H59.

The stable adsorption configurations of DPA at the optimal adsorption site H3-1 on the (001) surface of kaolinite and at the optimal adsorption site H2-1 on the (00$\bar{1}$) surface are shown in Fig. 6. The hydrogen bond analysis shows that on the (001) surface of kaolinite, DPA is mainly adsorbed by forming three hydrogen bonds through the O atoms in the molecule and the H atoms on the Al-OH group, namely O31-H33, O73-H22, and O74-H11. While on the (00$\bar{1}$) surface of kaolinite, it is mainly adsorbed by forming one hydrogen bond through the H atom in the DPA molecule and the O atom on the Si-O group, which is O28-H34.

Table 2. Adsorption energy of DDPA on the (001) and (00$\bar{1}$) surfaces of kaolinite

DDPA			Adsorption energy（kJ/mol）		
Adsorption site	001	00$\bar{1}$	Adsorption site	001	00$\bar{1}$
H1-1	-130.48	-31.08	H2-3	-112.23	-45.73
H1-2	-95.74	-30.16	H3-1	-122.53	-47.43
H1-3	-126.04	-31.68	H3-2	-99.23	-43.44
H2-1	-147.92	-42.20	H3-3	-96.59	-37.37
H2-2	-134.59	-44.03			

Table 3. Adsorption energy of DPA on the (001) and (00$\bar{1}$) surfaces of kaolinite

DPA			Adsorption energy（kJ/mol）		
Adsorption site	001	00$\bar{1}$	Adsorption site	001	00$\bar{1}$
H1-1	-140.9126	-45.32	H2-3	-81.18	-37.91
H1-2	-129.6518	-32.04	H3-1	-152.38	-35.09
H1-3	-124.5254	-29.16	H3-2	-137.82	-38.83
H2-1	-122.4806	-46.78	H3-3	-95.74	-28.72
H2-2	-139.1238	-31.92			

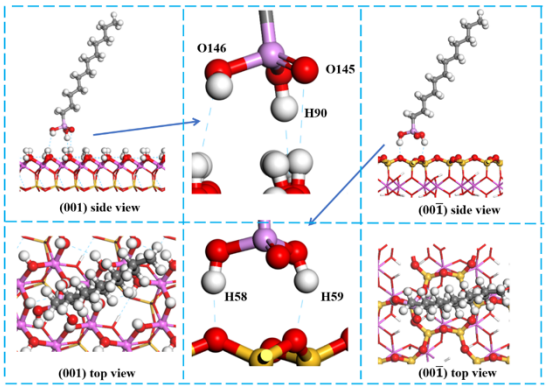

Fig. 5. The optimal adsorption configuration of DDPA on the surface of kaolinite

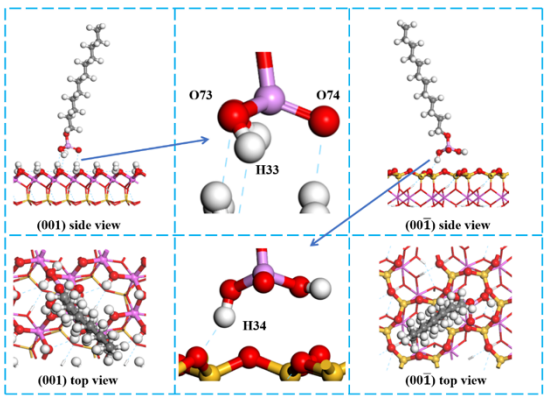

Fig. 6. The optimal adsorption configuration of DPA on the surface of kaolinite

4.1.2 . Analysis of differential electron density, Mulliken population and density of states

To further analyze the adsorption mechanism of DDPA and DPA on the AL-OH group of kaolinite (001) surface and the Si-O group of kaolinite ($00\bar{1}$), the differential electron density, Mulliken population and density of states analysis were carried out for the optimal adsorption configuration of the two agents on the kaolinite surface. Fig. 7 and 8 are the differential electron density diagrams of the adsorption of DDPA and DAP on the (001) surface and ($00\bar{1}$) surface of kaolinite. The blue area indicates the accumulation of electrons, and the yellow area indicates the consumption of electrons.

As shown in Fig. 7, obvious electron transfer exists on both the (001) surface and the ($00\bar{1}$) surface of kaolinite for DDPA. During the adsorption process of DDPA on the (001) surface of kaolinite, electrons mainly accumulate at the double-bond O atoms in the DDPA molecule, while during the adsorption process on the ($00\bar{1}$) surface, electrons mainly concentrate at the O atoms of the Si-O group. The electron transfer situation during the adsorption process of DPA on the (001) surface and the ($00\bar{1}$) surface of kaolinite is consistent with that of DDPA (Fig. 8).

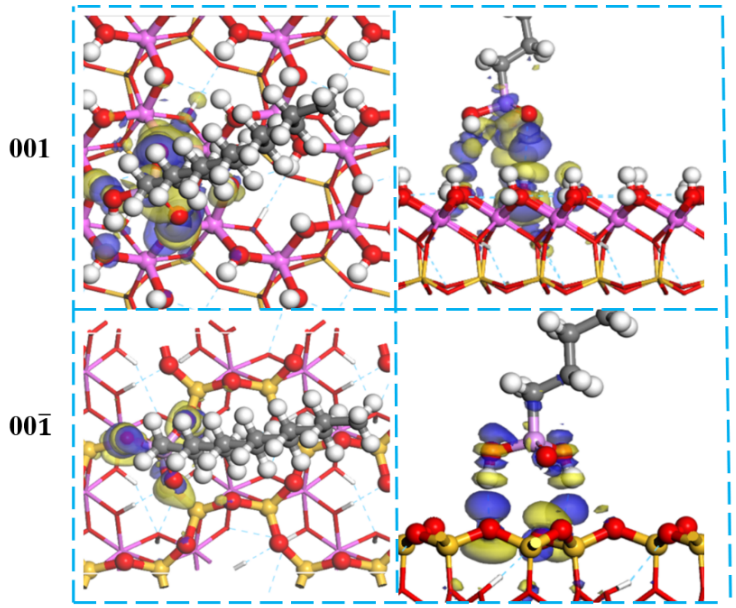

Fig. 7. The differential electron density map of DDPA adsorption on the surface of kaolinite

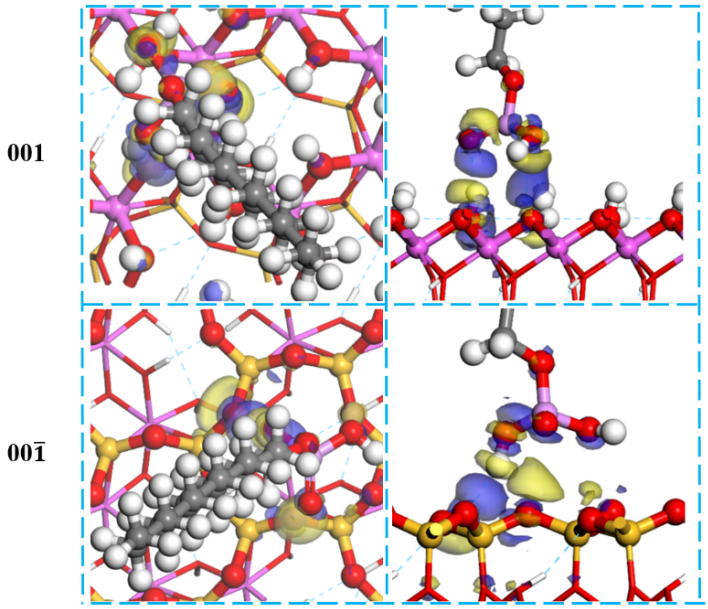

Fig. 8. The differential electron density map of DPA adsorption on the surface of kaolinite

Table 4. Mulliken charge transfer of the reagent before and after adsorption on the (001) surface of kaolinite

Collector type	Atom number	Adsorption State	Charge(e)	Transfer
DPA	O74	before	-1.00	0.04
		after	-0.96	
	H33	before	0.25	-0.25
		after	0.50	
	O73	before	-1.00	-0.02
		after	-1.02	
	H22	before	0.45	-0.02
		after	0.43	
	H11	before	0.45	-0.02
		after	0.43	
	O31	before	-1.06	0.02
		after	-1.04	
DDPA	O145	before	-1.00	-0.03
		after	-1.03	
	H90	before	0.25	-0.25
		after	0.50	
	O146	before	-0.99	0.04
		after	-0.95	
	H7	before	0.45	-0.02
		after	0.43	
	H3	before	0.41	-0.04
		after	0.45	
	O15	before	-1.06	0.06
		after	-1.00	

Table 5. Mulliken charge transfer of the reagent before and after adsorption on the (00$\bar{1}$) surface of kaolinite

Collector type	Atom number	Adsorption State	Charge (e)	Transfer (e)
DPA	O28	before	-1.14	0.01
		after	-1.13	
	H34	before	0.25	-0.25
		after	0.50	
DDPA	O39	before	-1.00	-0.13
		after	-1.13	
	H58	before	0.25	0.25
		after	0.50	
	O41	before	-1.00	-0.13
		after	-1.13	
	H59	before	0.25	0.25
		after	0.50	

Charge redistribution is one of the main reasons for the formation of hydrogen bonds. Therefore, in the study of the adsorption process of the reagent on the kaolinite surface, the charge distribution was used to study the charge redistribution of the single-bond O atoms, double-bond O atoms, and H atoms in the adsorption process. Tables 4 and 5 show the Mulliken charge transfer before and after the adsorption of the reagent on the (001) surface and (00$\bar{1}$) surface of kaolinite, respectively. It can be seen that when the reagent is adsorbed on the (001) surface of kaolinite, the double-bond O74 atom in DPA gains 0.04 e electrons after adsorption, the single-bond O73 atom loses 0.02 e, the H33 atom loses a total of 0.25 e, the O31 on the kaolinite surface gains 0.02 e, and both H22 and H11 lose 0.02 e; in DDPA, the

double-bond O145 atom loses 0.03 e electrons after adsorption, the single-bond O146 atom gains 0.04 e, the H90 atom loses a total of 0.25 e, the O15 on the kaolinite surface gains 0.06e, and H3 and H7 lose 0.04 e and 0.02 e, respectively; when the reagent is adsorbed on the $(00\bar{1})$ surface of kaolinite, the H34 atom in DPA loses 0.25 e electrons after adsorption, and the O28 on the kaolinite surface gains 0.01 e electrons; in DDPA, the H58 and H58 atoms gain 0.25 e electrons after adsorption, and the O39 and O41 on the kaolinite surface lose 0.13e electrons; It can be found that the adsorption of DDPA and DPA on the $(00\bar{1})$ surface of kaolinite mainly relies on hydrogen bonding, and the charge transfer of hydrogen bond-bonded atoms of DDPA on the $(00\bar{1})$ surface of kaolinite is more, indicating that the adsorption with quartz is better than that of DPA. The electron transfer between hydrogen bond donors and acceptors provides a theoretical basis for the formation of hydrogen bonds and the electrostatic interaction between the reagent and the mineral.

4.1.3. Mulliken population and PDOS analysis

According to the differential electron density of DDPA and DPA on the (001) and $(00\bar{1})$ surfaces of kaolinite and the Mulliken electron transfer situation, it can be found that the adsorption of the reagent on the mineral surface is mainly driven jointly by electrostatic interaction and hydrogen bonding interaction. Through the Mulliken population and PDOS analysis of hydrogen bonds of DPA and DDPA on the (001) surface of kaolinite and the $(00\bar{1})$ surface of kaolinite, combined with the adsorption energy results, the microscopic adsorption mechanism is revealed.

As shown in Table 6 and 7, they are the Mulliken population data of DDPA and DPA on the (001) and $(00\bar{1})$ surfaces of kaolinite, respectively. According to the bond population and bond length results, it can be known that the average bond population and bond length of DDPA on the (001) surface of kaolinite are 0.05 and 2.20598 Å, respectively, and on the $(00\bar{1})$ surface of kaolinite are 0.03 and 1.943875 Å, respectively. The average bond population and bond length of DPA on the (001) surface of kaolinite are 0.03 and 2.10533 Å, respectively, and on the $(00\bar{1})$ surface of kaolinite are 0.00 and 2.75849 Å, respectively. It can be found that the hydrogen bonds formed by DDPA and DPA on the (001) surface of kaolinite are both weak hydrogen bonds, and the covalency intensity of the hydrogen bonds is stronger than that of the $(00\bar{1})$ surface of kaolinite. Among them, the hydrogen bond strength and stability of DPA on the (001) surface of kaolinite are significantly higher than those of the $(00\bar{1})$ surface of kaolinite, and the hydrogen bond of DDPA on the $(00\bar{1})$ surface of kaolinite is stronger than that of DPA, providing a theoretical basis for achieving targeted adsorption of kaolinite in the kaolinite-quartz mixed mineral system.

Table 6. Mulliken population of the reagent on the (001) surface of kaolinite

Adsorption configuration	Bond type	Population	Length
DDPA	O145-H15	0.08	1.80824
	O146-H34	0.03	1.96126
	O84-H90	-0.01	2.84844
DPA	O31-H33	0.04	1.96424
	O73-H22	0.04	1.98202
	O74-H11	-0.02	2.36973

Table 7. Mulliken population of the reagent on the $(00\bar{1})$ surface of kaolinite

Adsorption configuration	Bond type	Population	Length
DDPA	O39-H58	0.04	1.88093
	O41-H59	0.02	2.00682
DPA	O28-H34	0	2.75849

The polar head groups of DDPA and DPA contain single-bonded O atoms, double-bonded O atoms, P atoms, and hydrogen atoms. To determine the activity of the bonding atoms of the double-bonded oxygen atoms in the collectors, the density of states of DDPA and DPA was calculated, and the

calculation parameters were consistent with the geometric structure optimization parameters. The results of the density of states analysis are shown in Fig. 9 to 12, and the Fermi level (Ef) value is set to 0 eV.

Through the PDOS analysis of the bonding atoms of DDPA and DPA on the (001) surface of kaolinite, it can be found that the electron density at the Fermi level (Ef) of the bonding atoms after the adsorption of DDPA on the (001) surface of kaolinite has decreased significantly, and both the antibonding and bonding orbits have undergone orbital hybridization, further indicating the formation of hydrogen bonds, and the O-2p and H1s orbits are the main contributing orbits. At the same time, both the hydrogen bonds O146-H34 and O145-H15 have a new peak formation in the energy band of 0 - 5 eV. Combined with the adsorption energy results, it can be concluded that the adsorption process of DDPA and DPA on the (001) surface of kaolinite is mainly driven by the synergy of electrostatic interaction and hydrogen bond interaction. Meanwhile, after the adsorption of DPA on the (001) surface of kaolinite, the electron density of the hydrogen bond (O73-H22) at Ef increases (Fig. 12), and the bond population value is positive, indicating that this hydrogen bond can provide more coordination electrons for the entire adsorption process, which is conducive to the stability of the adsorption configuration. Moreover, obvious orbital hybridization also occurs in both the bonding and antibonding orbits, and the formed new peaks are also in the energy band of 0 - -5 eV, and the O-2p and H1s orbits are the main contributing orbits, indicating that the adsorption between DPA and the (001) surface of kaolinite is also mainly driven by the synergy of electrostatic interaction and hydrogen bond interaction.

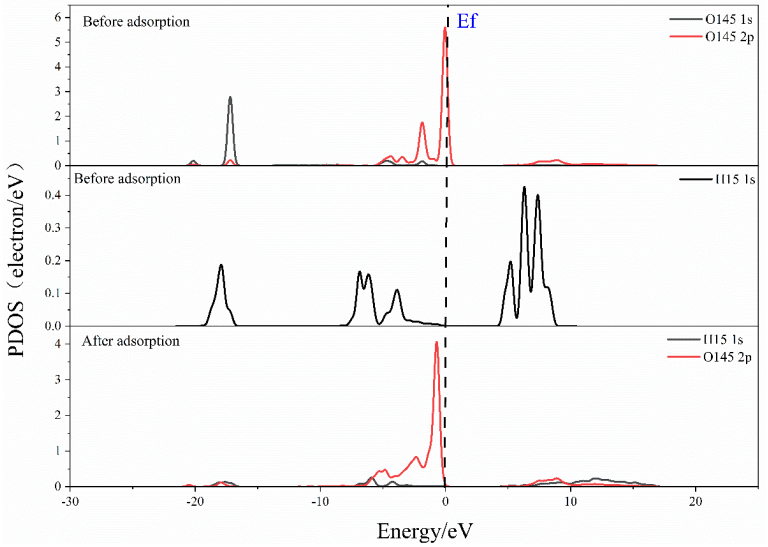

Fig. 9. The density of electronic states of the double bond O atoms in DDPA before and after adsorption on the (001) surface of kaolinite

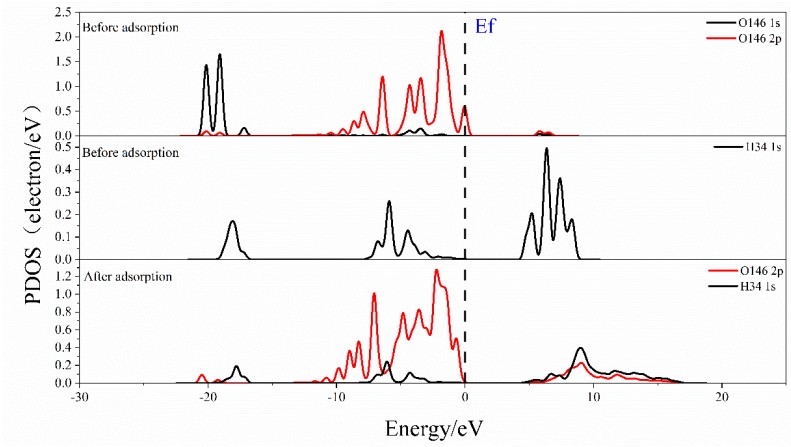

Fig. 10. The density of electronic states of the single-bonded O atom in DDPA before and after adsorption on the (001) surface of kaolinite

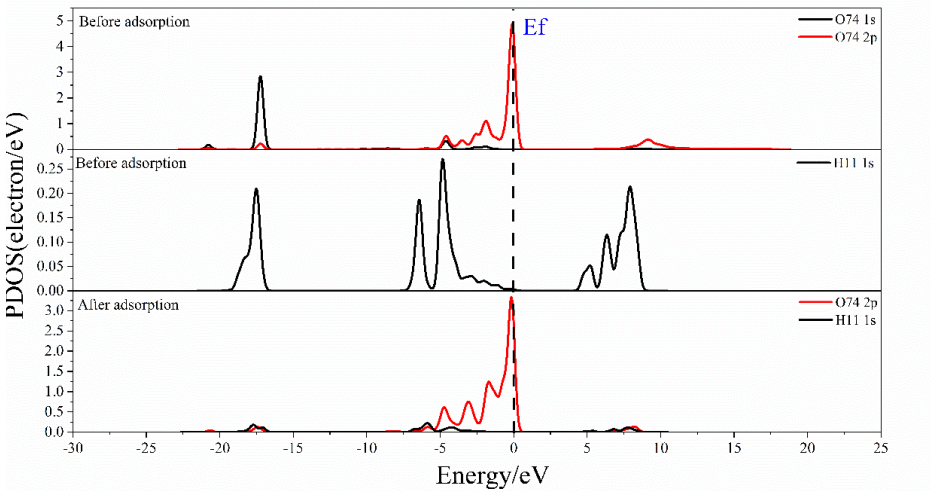

Fig. 11. The density of electronic states of the double-bond O atoms in DPA before and after adsorption on the (001) surface of kaolinite

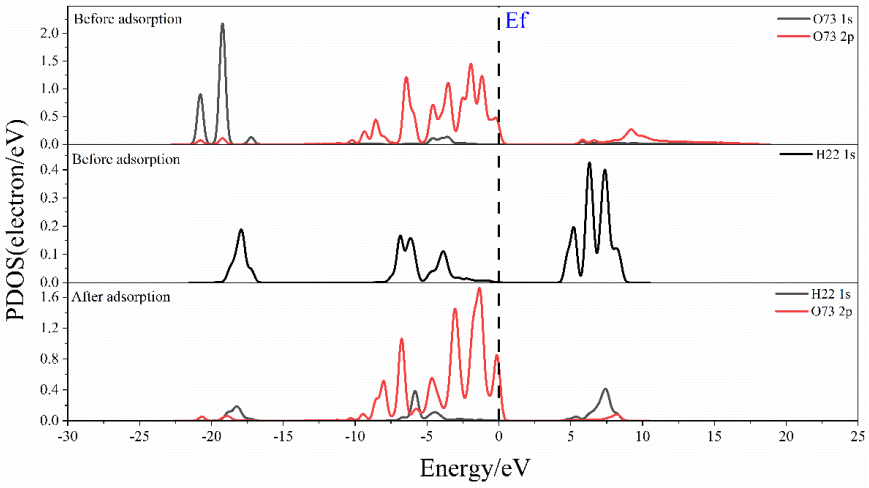

Fig. 12.The density of electronic states of the double-bonded O atoms in DPA before and after adsorption on the (001) surface of kaolinite

4.2. Experimental verification

4.2.1. Fourier transform infrared spectroscopy analysis

At present, it is difficult to directly verify the adsorption differences of the reagent on the kaolinite (001) surface and the kaolinite (00$\bar{1}$) surface by experimental means. Since the quartz mineral is similar to the kaolinite (00$\bar{1}$) surface structure in crystal structure, both have Si-O basal planes. Therefore, the paper used quartz and kaolinite minerals for infrared spectral analysis after reagent adsorption, and carried out flotation tests of single minerals and mixed minerals, respectively, to verify the previous simulation results.

The infrared spectra of DDPA and DPA before and after adsorption on the surfaces of kaolinite and quartz are shown in Fig. 13 and 14. It can be seen that no new peaks appeared on the surfaces of kaolinite and quartz after the adsorption of the reagents, indicating that only physical adsorption occurred. Among them, after the interaction of DPA, DDPA and kaolinite, compared with the spectrum of kaolinite itself, there were shifts at 3692 and 915 cm^{-1}, corresponding to the stretching vibration peak of Al-OH and the vibration of the Al-O-P bond, respectively, indicating that the reagents were adsorbed on the surface of kaolinite (Guo et al., 2021); after the interaction of DPA, DDPA and quartz, compared with the spectrum of quartz itself, there were shifts at 3437 and 2921 cm^{-1}, corresponding to the stretching vibration of -OH of quartz and water and the stretching vibration of C-H in the alkyl chain,

respectively. After the interaction of DPA, DDPA, and quartz, it shifted to a lower frequency at about 1080 cm^{-1}, indicating that the physical adsorption of the reagent on the quartz surface caused the shift of the Si-O peak. Among them, after the interaction of kaolinite and the reagent, compared with its spectrum, the peak change at Al-O-P is a key sign of the specific adsorption of the reagent on the surface of kaolinite; after the interaction of quartz and the reagent, only weak physical adsorption occurred, and there was no specific chemical bonding. This result provides an experimental basis for the selective separation of kaolinite by phosphonic acid collectors in highly argillaceous coal slime water.

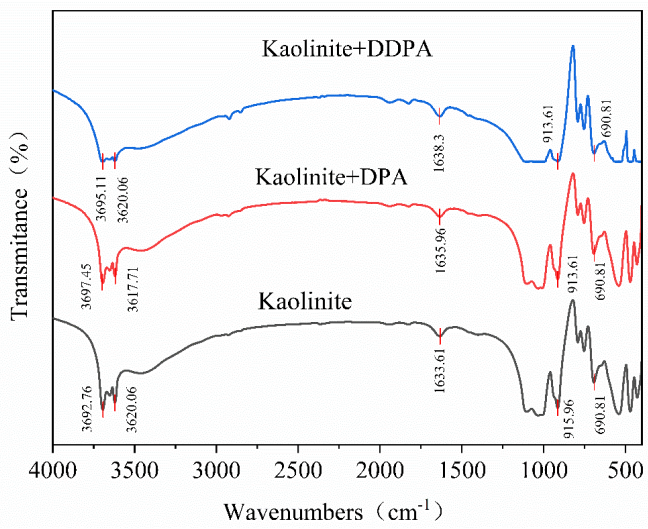

Fig. 13. Infrared spectra of DDPA and DPA before and after interacting with kaolinite (reagent concentration: 3 mmol/L)

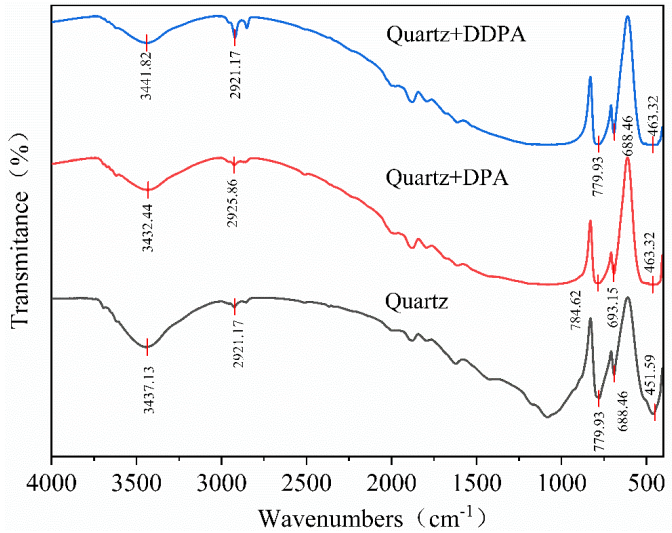

Fig.14. Infrared spectra of DDPA and DPA before and after interaction with quartz (reagent concentration: 3 mmol/L)

4.2.2. Single mineral flotation test

The flotation characteristics of kaolinite and quartz minerals with DDPA and DPA at the natural pH value were studied, and the results are shown in Figure 15. It can be seen that when the mineral particle size is less than 125 μm, the adsorption effect of DPA on kaolinite and quartz is better than that of DDPA. However, when the concentration of DDPA is around 1 mmol/L, the flotation effect on minerals is almost zero, while DPA still has a strong adsorption effect on kaolinite at a lower concentration. As shown in Figure 16, when the reagent concentration is less than 1 mmol/L, DPA has a strong difference in the recovery performance of 125-75 μm kaolinite and quartz. Therefore, at low concentrations, DPA

is more likely to adsorb on the surface of kaolinite than DDPA. At high concentrations, the difference in the recovery performance of DAP and DDPA on kaolinite and quartz decreases. When the reagent concentration is greater than 2 mmol/L, the collection difference of DPA on kaolinite and quartz changes, and its collection performance on kaolinite is weaker than that of DDPA.

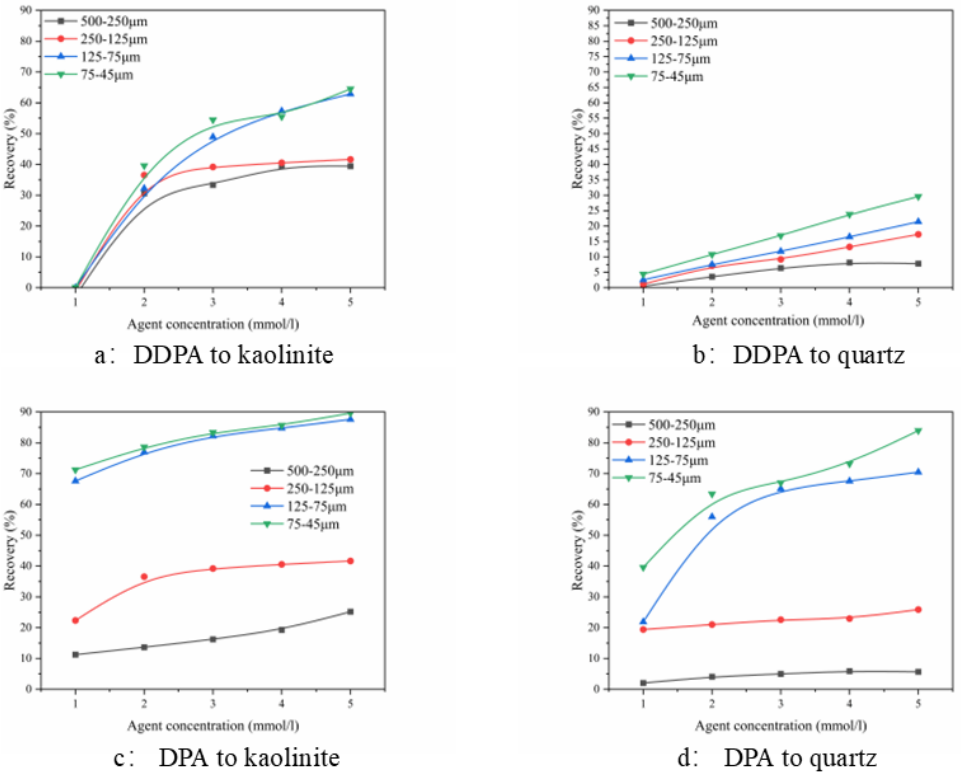

Fig. 15.The flotation performance of DDPA and DPA on kaolinite and quartz particles of different particle sizes

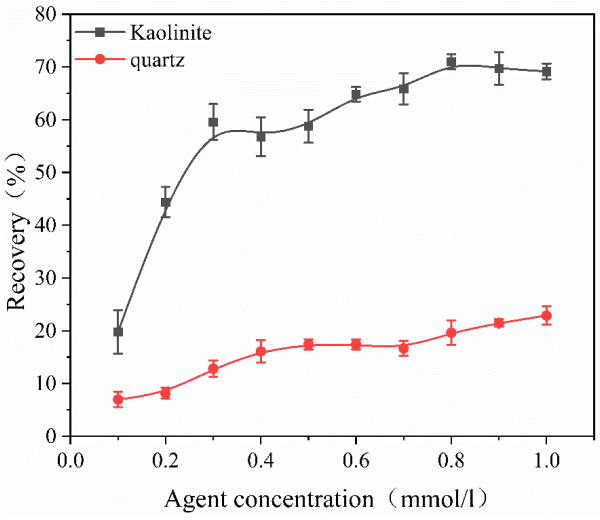

Fig. 16.The influence of DPA concentration on the recovery rates of 125 - 75 μm kaolinite and quartz

4.2.3. Flotation test of mixed minerals

According to the flotation results of single minerals, the DPA reagent was selected in this paper, and the flotation test of kaolinite-quartz mixed minerals with a particle size of 125-75 μm was carried out. The results are shown in Table 8.

Table 8. Test results of flotation separation of DPA and kaolinite-quartz (125 - 75 μm) mixed minerals under different concentrations

Agent	Agent concentration (mmol/L)	Al_2O_3/SiO_2 (%)	Separating efficiency（%）
DPA	1	54.32	68.62
	2	52.75	67.05
	3	49.11	63.41
	4	44.98	59.28
	5	44.66	58.96

It can be seen that when the mineral particle size is within 125 - 75 μm, in the kaolinite-quartz mixed mineral system of DPA, when the reagent concentration is 1 mmol/L, the selective adsorption effect on kaolinite is the best, and the separation efficiency is 68.62%. With the increase of the concentration, the selective adsorption effect on kaolinite gradually decreases. When the reagent concentration is 5 mmol/L, the separation efficiency is 58.96%, which is consistent with the results of the single mineral flotation test. At the same time, it also indicates that the adsorption effect of DPA on the (001) surface of kaolinite is stronger than that on the $(00\bar{1})$ surface of kaolinite.

5. Conclusion

(1) According to the results of DFT simulation calculations, it can be known that the adsorption of the two agents on the (001) surface of kaolinite is mainly driven by the synergy of electrostatic interaction and hydrogen bonding. The adsorption on the $(00\bar{1})$ surface of kaolinite is mainly due to hydrogen bonding, and the order of adsorption strength is: DPA/kaolinite(001) > DDPA/kaolinite(001) > DDPA/ kaolinite$(00\bar{1})$ > DPA/ kaolinite$(00\bar{1})$.

(2) FTIR and flotation test results confirm the presence of hydrogen bonding interactions between both DDPA and DPA with kaolinite and quartz surfaces. At lower DPA concentrations (<1 mmol/L), a pronounced selective collection effect toward kaolinite is observed. Within the 0.3-1 mmol/L range, the recovery of kaolinite reaches 63.35%-67.59%, while quartz recovery remains low at 12.76%-21.87%. In mixed mineral flotation, DPA also shows selectivity for kaolinite at the 125-75 μm particle size range. These experimental findings are highly consistent with the simulation results.

(3) The strong agreement between DFT simulations and experimental results confirms the feasibility of using the kaolinite $(00\bar{1})$ surface as a substitute for quartz in adsorption modeling.

Acknowledgements

This work was supported by the Natural Science Foundation of China [grant number 52174232].

References

ALI A M., PADMANABHAN E., MIJINYAWA A., 2019, *Effect of pH on the stability of quartz in a multi-phase system of kaolinite, hydrous Al (hydr) oxide and quartz,* SN Applied Sciences, 1, 1-11.

ALVAREZ-COSCOJUELA A., MAÑOSA J., FORMOSA J., 2024, *Structural characterisation and reactivity measurement of chemically activated kaolinite,* Journal of Building Engineering, 87, 109051.

BECHTHOLD, P., JUAN, J., JUAN, A., MARCHETTI, J.M., 2024, *The adsorption of ethyl formate on CaO: A DFT study*. J. Phys. Chem. Solids, 185, 111780.

CHEN, S., YANG, Z., WANG, F., 2019. *Preparation and characterization of polyimide/kaolinite nanocomposite films based on functionalized kaolinite*, Polymer Engineering & Science, 59(s2), E380-E386.

CHI, Q., ZHEN, R., WANG, X., 2017, *The role of exfoliated kaolinite on crystallinity, ion conductivity, thermal and mechanical properties of poly (ethylene oxide)/kaolinite composites*, Polymer Bulletin, 74, 3089-3108.

CLARK S J., SEGALL M D., PICKARD C J., 2005, *First principles methods using CASTEP*, Zeitschrift für kristallographie-crystalline materials, 220(5-6), 567-570.

GUO, F., ZHOU, M., XU, J., 2021, *Glyphosate adsorption onto kaolinite and kaolinite-humic acid composites: experimental and molecular dynamics studies,* Chemosphere, 263, 127979.

HOU, B., LIU, L., 2020,*Study on the influence of Ca^{2+} in sodium oleate system on the flotation of kaolinite and quartz at different pH values* , Coal Engineering, 52, 149-154.

KAMACHI, T., TATSUMI, T., TOYAO, T., HINUMA, Y., MAENO, Z., TAKAKUSAGI, S., FURUKAWA, S., TAKIGAWA, I., SHIMIZU, K.-I., 2019, *Linear correlations between adsorption energies and HOMO levels for the adsorption of small molecules on TiO_2 surfaces*. J. Phys. Chem. C, 123(34), 20988–20997.

LI, Y., HOU, D., DING, X., 2023. *Influence of coal-measure kaolinite with different types on the preparation of kaolinite nanotub,* Applied Clay Science, 246, 107179.

LIU, B.-J.-M., LEI, X.-T., AHMADI, M., CHEN, Z., 2024, *Molecular insights into oil detachment from hydrophobic quartz surfaces in clay-hosted nanopores during steam-surfactant co-injection*. *Pet. Sci.*, 21(4), 2457–2468.

LIU, L., SHEN, L., LI, W.,2018, *Study on the aggregation behavior of kaolinite particles in the presence of cationic, anionic and non-ionic surfactants*, Plos one, 13(9), e0204037.

LIU, J., WANG, X., LIN, C, L., 2015, *Significance of particle aggregation in the reverse flotation of kaolinite from bauxite ore*, Minerals Engineering, 78, 58-65.

LIU, L., KONG, C., ZHAO, H., 2024, *Elucidating the enhancement of kaolinite flotation by iron content through density functional theory: A study on sodium oleate adsorption efficiency,* International Journal of Mining Science and Technology, 34(6), 855-866.

LIU, W., LIU, W., ZHAO, B., 2019, *Novel insights into the adsorption mechanism of the isopropanol amine collector on magnesite ore: A combined experimental and theoretical computational study*, Powder Technology, 343, 366-374.

LU, F., LIU, L., KONG, C., ZHAO, H., 2024, *Enhancing coal slime processing: Investigating the efficacy of sodium dodecyl sulfonate in the adsorption on kaolinite surfaces*. Asia-Pac. J. Chem. Eng., 19(4), 3047.

LONGHUA, X., YUEHUA, H., FAQIN, D., 2015, *Effects of particle size and chain length on flotation of quaternary ammonium salts onto kaolinite*, Mineralogy and Petrology, 109, 309-316.

MA C., ABULIKEMU A., BAO J., 2023, *Stacking Order Induced Anion Redox Regulation for Layer-Structured Na0. 75Li0. 2Mn0. 7Cu0. 1O2 Cathode Materials*, Small, 19(37), 2302332.

MA X., BRUCKARD W J., HOLMES R., 2009, *pH and ionic strength on the cationic flotation of kaolinite*, International Journal of Mineral Processing, 93(1), 54-58.

MORSY F A., EL-SHERBINY S., HASSAN M S., 2014, *Modification and evaluation of Egyptian kaolinite as pigment for paper coating*, Powder technology, 264, 430-438.

MÜLLER A S., JANJIĆ K., SHOKOOHI-TABRIZI H., 2020, *The response of periodontal cells to kaolinite*, Clinical Oral Investigations, 24, 1205-1215.

PRATES, L.M., SILVA, L.A., PEREIRA, A.M., CORREIA, J.C.G., MARQUES, M.L.S., FILIPPOVA, I.V., FILIPPOV, L.O., 2025, *Reverse flotation of iron ore by a new ternary collector-frother reagent: Fundamentals of adsorption from spectroscopy and molecular modeling*. Appl. Surf. Sci., 682, 161609.

SEGALL M D., LINDAN P J D., PROBERT M J., 2002, *First-principles simulation: ideas, illustrations and the CASTEP code*, Journal of physics: condensed matter, 14(11), 2717.

ŠOLC R., GERZABEK M H., LISCHKA H., 2011, *Wettability of kaolinite (001) surfaces – Molecular dynamic study*, Geoderma, 2011, 169: 47-54.

SPRANKLE P., MEGGITT WF., PENNER D.,1975, *Adsorption, Mobility, and Microbial Degradation of Glyphosate in the Soil*, Weed Science, 23(3), 229-234.

YANG, S., FENG, Q., QIU, X., 2014. *Relationship between flotation and Fe/Mn ratio of wolframite with benzohydroxamic acid and sodium oleate as collectors*, Journal of Physicochemical Problems of Mineral Processing, 50, 747-758.

ZHANG, H., XU, Z., SUN, W., ZHU, Y., CHEN, D., ZHANG, C., 2023, *Hydroxylation structure of quartz surface and its molecular hydrophobicity*. Appl. Surf. Sci., 612, 156056.

ZHANG, B., GUO, H., DENG, L., 2020, *Undehydrated kaolinite as materials for the preparation of geopolymer through phosphoric acid-activation,* Applied Clay Science, 199, 105887.

ZHOU,C., LIU.,L, CHEN,J., 2022.Study on the influence of particle size on the flotation separation of kaolinite and quartz. Journal of Powder Technology, 408,117747.